A major purpose of the Technical Information Center is to provide the broadest dissemination possible of information contained in DOE's Research and Development Reports to business, industry, the academic community, and federal, state and local governments.

Although a small portion of this report is not reproducible, it is being made available to expedite the availability of information on the research discussed herein.

1

LA-UR -86-300

CONF-851053--9

Los Alamos National Laboratory is operated by the University of California for the United States Department of Energy under contract W-7405-ENG-36

LA-UR--86-300

DE86 006033

TITLE: ANALYSIS, MODELING, AND DESIGN OF SHORT-WAVELENGTH LASER-PLASMA EXPERIMENTS

AUTHOR(S): W. C. Mead, S. V. Coggeshall, S. R. Goldman, E. K. Stover, P. D. Goldstone, A. Hauer and J. M. Kindel, Los Alamos National Laboratory, L. Montierth, University of Arizona

SUBMITTED TO: For the Proceedings of the 7th International Workshop on Laser Interaction and Related Plasma Phenomena, October 28 - November 1, 1985 in Monterey, California.

DISCLAIMER

Los Alamos Los Alamos National Laboratory
Los Alamos, New Mexico 87545

ANALYSIS, MODELING, AND DESIGN OF SHORT-WAVELENGTH LASER-PLASMA EXPERIMENTS

W. C. Mead, S. V. Coggeshall, S. R. Goldman, E. K. Stover,
P. D. Goldstone, A. Hauer, and J. M. Kindel

Los Alamos National Laboratory
Los Alamos, N.M. 87545

L. Montierth

University of Arizona
Tucson, AZ 85721

ABSTRACT

We present analysis and LASNEX modeling of two experiments designed to explore the mechanisms and scaling of laser-plasma coupling in high-Z plasmas. The first used layered Au-on-CH spheres irradiated symmetrically using the Omega (Laboratory for Laser Energetics) 0.35 μm laser to observe the x-ray emission and energy penetration in gold plasmas. Measurements of the subkilovolt and kilovolt emission from targets with varying Au-coating thicknesses were made using diagnostics of varying spectral, temporal, and spatial resolution. The results indicate that the x-ray conversion efficiency is a function of target size, with larger targets yielding x-ray emission in excellent agreement with calculations. The x-ray emission fall-off with decreasing gold thickness agrees well with predictions. The second experiment used the Novette (Lawrence Livermore National Laboratory) laser to irradiate solid gold disk targets, examining wavelength scaling to 0.26 μm. The measured subkilovolt x-ray emission is in good agreement with calculations using mildly inhibited thermal electron transport, indicating enhanced target coupling, compared with previous experiments using smaller spot sizes. The experiment also indicates very low suprathermal electron populations, on the order of 0.1% at about 30 keV effective temperature. Finally, we present preliminary plans and designs for experiments which will use the Aurora 5 kJ, 5 ns, 0.25 μm KrF laser now being constructed at Los Alamos.

I. INTRODUCTION

As the severe drawbacks of using the 10.6 μm light from the CO_2 laser have become increasingly apparent, Los Alamos has been more and more strongly attracted by the benefits of the 0.25 μm KrF laser system as a potential Inertial Confinement Fusion (ICF) driver. The work reported here is a subset of the growing Los Alamos program to investigate and exploit the advantageous laser-plasma coupling available at short laser wavelengths. This program of theory and experiment is coupled with a strong program to conceive, design, and build a gas excimer (KrF) laser system capable of meeting the stringent requirements of ICF.

In this paper, we report analysis of two experiments designed to extend our knowledge[1,2] of the coupling of short-wavelength laser light to high-Z plasmas: the "High-Z Plasma Dynamics Experiment" and the "Gold-Disk 0.26 μm Scaling Experiment". We also present initial plans and designs for experiments which will use the Aurora prototype KrF laser system now being built at Los Alamos.

As background, Fig. 1 shows a summary of x-ray conversion efficiency data as of about 1983, the start of this work. The x-ray conversion efficiency is predicted to increase as $I\lambda^2$ decreases. The measured conversion efficiencies agree very well (for the higher intensity, longer wavelength points) with the power-law fit to LASNEX calculations using inhibited electron transport (f_s=0.03). However, at lower intensities and shorter wavelengths, the measured conversion efficiency is below that predicted by as much as 50%. In the case of such a discrepancy with modeling, the correct scaling parameter is uncertain. In particular, depending upon the mechanism, the x-ray conversion deficit could be dependent on the intensity and the laser wavelength to different degrees, or perhaps upon other parameters, as well. Thus, previous work raised two important questions: (1) What mechanisms are responsible for the x-ray conversion deficit for low-intensities and/or short-wavelengths? and (2) Does the discrepancy present significant scaling difficulties for the 0.25 μm wavelength of the KrF laser? The two experiments analyzed here address these questions.

Figure 2 shows calculations indicating the relevant physics in the discrepant (low-intensity) and non-discrepant (high-intensity) regimes. At low intensities, the underdense plasma can radiate rapidly enough to remove the deposited laser energy locally. This results, calculationally, in a cool corona with an extended absorption and emission region. Calculated x-ray conversion efficiencies are quite high. At higher intensities, the radiation from the underdense plasma can no longer cool the corona as rapidly as the laser deposits its energy. As a result, the corona becomes hotter and electron transport carries the energy into the overdense plasma where radiation processes are more rapid. Since the laser deposits its energy via Inverse Bremsstrahlung most efficiently near the critical surface, and the electron mean free paths are short, the plasma becomes quite steep near critical. The higher corona temperatures and the steeper gradients increase the energy transfer to plasma blow-off, while the need to transport energy into the overdense plasma before it can radiate further reduces the energy available for radiation. Thus the x-ray conversion efficiency is reduced at

higher intensities.

These qualitative differences in plasma profiles lead to a number of observable signatures. The increase in corona' temperature at high intensity leads to increased average ionization state and increased emission from the gold M-lines in the spectral region around 2.5 keV. The spatial extent (normal to the target surface) of the x-ray emission is predicted to be smaller for the steeper, high-intensity profiles. Energy penetration into the plasma is greater for the higher intensity case. For example, the material depth (referenced to gold at solid density) to which the laser light penetrates at the peak of the pulse is about 400 Å at $4x10^{14}$ W/cm^2 and about 870 Å at $4x10^{15}$ W/cm^2. Finally, in the high intensity case, a sharp decrease in the emission from a layered Au-on-CH target might be observable as the laser burns through the gold layer. These predictions have been tested in the High-Z Plasma Dynamics Experiment.

The model assumptions used in the LASNEX[3] calculations presented here correspond closely with those used previously.[1,2] The dominant processes in high-Z laser-plasma coupling are hydrodynamics, laser absorption via Inverse Bremsstrahlung, and non-LTE atomic and radiation physics. For the higher irradiation intensities, electron thermal conduction becomes important as a mechanism to transport the deposited energy into the overdense plasma. For this work, thermoelectric magnetic fields and multigroup hot electron modeling were excluded from the LASNEX modeling. Previous work[2] indicates that these features play modest roles in determining the overall energetics and conditions of high-Z, short-wavelength laser-produced plasmas.

The two experiments presented here provide complementary views of the physics of high-Z plasmas. The experiments are quite similar in most irradiation parameters and both use a comprehensive array of diagnostics, particularly for the soft x-ray emission. There are two significant differences between the experiments. The first is geometry: the Plasma Dynamics Experiment[4] used spherical geometry and relatively uniform illumination, while the 0.26 μm Scaling Experiment[5] used planar geometry. For spheres, the angular integration to obtain total x-ray conversion is simple and beam-edge effects should be negligible. For planar targets, the x-ray conversion is inferred from angular distribution measurements[2] or from single-angle measurements together with 2D calculations, as in this work. Also, for the same laser energy, pulse duration, and intensity, the plasma scalelength in spherical irradiations is smaller, as a result of the smaller characteristic length (radius) and the enhanced divergence of the plasma blow-off for spherical targets. The second major difference is that the Plasma Dynamics Experiment used layered Au-on-CH targets to probe energy penetration and emission as a function of depth into the material, while the 0.26 μm Scaling Experiment emphasized scaling of global variables for solid targets.

In the remainder of this paper, we discuss the High-Z Plasma Dynamics Experiment (II); the Gold Disk 0.26 μm Scaling Experiment (III); Plans and Designs for Aurora KrF Experiments (IV); and our Summary and Conclusions from this work (V).

II. HIGH-Z PLASMA DYNAMICS EXPERIMENT

The High-Z Plasma Dynamics Experiment[4] used Au-on-CH layered spheres to probe energy penetration and x-ray generation processes. The experiment was performed in collaboration between Los Alamos and the University of Rochester Laboratory for Laser Energetics, using the Omega laser. Highlights of the experiment are shown in Fig. 3. We have performed two experimental shot sequences: the first using 6 beams from Omega at low energies and using small target spheres; the second using 24 beams, providing higher-energy irradiations with greater spherical symmetry and using larger targets to obtain a given intensity. In each sequence, targets with varying gold-layer thickness were used to observe the material depth to which energy penetrates (and from which x-rays are emitted) in the high-Z plasma.

Using thick gold coated spheres, we measured the subkilovolt x-ray emission. The total x-ray conversion efficiencies (x-ray energy radiated/laser energy absorbed) plotted in Fig. 4 have been inferred from four-channel X-Ray Diode detectors using various unfold techniques. The initial experiments using 6 beams yielded x-ray conversion efficiencies which agreed very well with the earlier Argus experiments,[2] i.e. 60% and independent of intensity. This series, like earlier experiments, indicated an intensity-dependent discrepancy with calculations.

We subsequently repeated the experiment using 24 beam irradiations, which utilized higher energy, larger targets, and provided better illumination symmetry, but were otherwise like the 6-beam irradiations. The main goal was to use enhanced diagnostics on the experiment. To our surprise, the measured conversion efficiency increased, particularly at lower intensities. Examination of individual detector signals substantiates the inferred increase in emission levels for low intensity irradiations as the laser energy and target size increased. The recent 24-beam results are in excellent agreement with LASNEX calculations using slight electron transport inhibition (f_e=0.08).

The thin Au-coated targets allowed us to probe, for the first time, the depth to which energy penetrates and from which x-ray emission is produced. X-ray conversion efficiency decreases as the gold layer thickness decreases, since the emitting gold region is replaced by CH as the laser penetrates deeper into the material during the laser pulse. The observed fall-off of x-ray emission (Fig. 5) agrees well with LASNEX predictions, indicating that energy penetration into the target is well-calculated.

X-ray images of the targets show strong spatial modulation of the emission (Fig. 6). These images, obtained from 6-beam irradiations, show large-scale structures caused by non-uniformities from imperfect beam overlap. A small-scale filamentary structure is particularly visible for targets with thin gold coatings. It is possible that the same structure is present for the thicker-coated targets, but somewhat masked by emission from the higher density gold plasma. The appearence of filamentary structures is fairly common in laser-produced plasmas[6] and suggests that processes such as laser-light filamentation[6] (thermal or ponderomotive), thermal[7] and/or radiative-cooling[8] instabilities might be operating. Beam- or target-surface- structures might also be

playing a role.

Traces of the x-ray images (Fig. 7) show emission profiles which resemble those calculated. The limb's brightness (relative to the central emission) and its spatial extent correspond reasonably well with calculations. Further comparisons with other shots are needed to determine repeatability and the role of illumination and emission inhomogeneities.

A Transmission Grating Spectrograph (GS) was employed to obtain fairly high resolution emission spectra for the subkilovolt x-rays. Figure 8 shows a LASNEX-calculated spectrum together with two GS spectra, one for a thick-Au-coated target, the other for a thin-coated target. The GS spectra differ significantly from the broad-band spectra discussed below (Fig. 13). The measured spectrum shows stronger-than-calculated O-manifold emission, suggesting deficiencies in detail of the atomic physics modeling. In particular, dielectronic recombination, which is omitted from the LASNEX modeling, might be expected to soften the spectrum as observed.

The kilovolt x-ray line emission indicates the ionization state of the warm parts of the plasma. Two typical spectra are shown in Fig. 9. The increased M-line emission in the 2-3 keV spectral region at higher laser intensities indicates stronger ionization of the plasma, generally as predicted by the LASNEX modeling.

The Plasma Dynamics Experiment has extended our knowledge of the mechanisms and behavior of x-ray production in high-Z plasmas. Measured x-ray conversion efficiencies agree with calculations at moderate-to-high intensities, for all target sizes. At low intensities, the discrepancy between measurements and calculations now appears to be target-size dependent, with large targets yielding emission which agrees quite well with calculations. We have determined, for the first time, that the material depth of energy penetration and x-ray emission is in excellent agreement with LASNEX predictions.

Certain features of the experiment are not reproduced by the modeling, and need to be examined further. The x-ray conversion efficiency at low intensities is not accurately tracked at small target sizes. The observed subkilovolt x-ray spectrum appears softer than calculated by LASNEX. We have obtained detailed measurements of the temporal profiles of the x-ray emission pulses, and these need further analysis. Further, details of the x-ray images and the spatial modulation should be examined. These observations should provide ample stimulation for future work.

III. GOLD DISK 0.26 μm SCALING EXPERIMENT

Los Alamos has provided analysis and simulations for the Gold Disk 0.26 μm Scaling Experiment[5] performed at Lawrence Livermore National Laboratory. This experiment provides the first high-energy laser-plasma coupling data for 0.26 μm laser light. For this work, Novette was configured to produce 0.5-1.6 kJ of light at the fourth harmonic of the Nd:glass laser. The irradiation wavelength is nearly equal to that of the KrF laser, although detailed differences between the beam properties of

the two lasers may exist (e.g. beam quality and bandwidth). The scheme of the 0.26 μm Scaling Experiment is shown in Fig. 10. Note particularly the single-beam, planar geometry and the single-angle x-ray emission measurements. The 5 μm-thick gold disk targets were generally tilted to permit the soft x-ray diagnostics to view the target surface at 60° to the normal. The laser was incident at 30° to the normal.

A snapshot of a representative LASNEX 2D calculation used to infer global energetics from the single-angle x-ray emission measurements is shown in Fig. 11. The laser, represented in the calculation by 100 to 400 rays, is incident from the right. Little energy is transported laterally by conduction in this calculation at short wavelength. However, the hydrodynamic expansion does proceed radially, in part, increasing the volume of the corona and reducing the coronal temperatures, compared with 1D calculations using the same initial laser spot size. The peak electron temperature in the plasma is 4.8 keV in this 2D calculation. This calculation and one at $4x10^{13}$ W/cm^2 show that the total radiated energy is 2π times the fluence at 60°to the target normal, to within a few per cent.

Hard x-ray spectra indicate the behavior of the energetic electrons in the plasma. In this experiment, the observed hard x-rays (Fig. 12) imply relatively low coronal temperatures and very low suprathermal electron populations. At low irradiance, no suprathermal tail is evident, and the observed thermal tail appears to be extremely soft, roughly as calculated. At high irradiance, the suprathermal tail suggests a 28 keV electron population containing of order 0.1% of the incident energy.

One of the outstanding discrepancies of this experiment is seen in the calculated excess of 10-50 keV x-ray emission for the higher intensity irradiations (Fig. 12b). LASNEX generates these x-rays from the tail of the coronal "thermal" electrons, under the (perhaps oversimplified) assumption of a Maxwellian distribution. Since these electrons are at several kT, significant deviations from a Maxwellian could sharply reduce the electron populations in this energy range. Such deviations have been suggested due to nonlinear Inverse Bremsstrahlung[9] and to effects of transport.[10] Since the hard x-ray spectrum is depressed so strongly, and the hard x-ray emission is not very sensitive to modifications of transport, an underpopulation of the electron tail by the laser absorption appears quite likely. We estimate $Z(v_o/v_e)^2$ is about 0.4 for the high intensity irradiations, a regime where this effect is predicted to occur.

The broad-band subkilovolt spectrum inferred from the Dante 10-channel X-Ray Diode detector system is shown in Fig. 13. The experimental unfold is in good agreement with the LASNEX calculations using f_e=0.05. Differences between the unfolded XRD spectrum and the high resolution grating spectrograph results discussed earlier (Fig. 6) should be investigated further.

The measured and calculated x-ray emission levels, integrated over the frequency range of 0. to 1.8 keV, at 60° to the target normal are plotted in Fig. 14. The results of this experiment are best fit using f_e=0.05, the same value which best matched the spectrum. The data points at high intensity might need a small correction (now being evaluated, but probably less than 10%) to adjust for the effects of the M-line emission

on the Dante XRD signals. The calculated conversion efficiencies shown here include the M-line emission, 1% and 10% of the total emission, respectively, at $9x10^{13}$ and $2x10^{15}$ W/cm^2.

The use of f_e=0.05 produces only slight thermal transport inhibition, even for the high intensity irradiations. We find that f_e=0.03, inferred from the analysis of previous high-Z disk irradiations,[1,2] yields a poorer match to both the x-ray spectrum and the absolute emission levels at high irradiation intensities for the present experiment. This suggests that, as experiments move towards shorter wavelengths and higher laser energies, whatever mechanisms were responsible for the inferred transport inhibition are becoming less important. The transport appears to be approaching "classical" levels, a trend also appearing in recent low-Z experiments.[11] This trend is at least plausible, given the increased collisionality, longer scalelengths, and reduced suprathermal electron populations encountered at higher laser energies and lower $I\lambda^2$

Figure 15a shows the incident laser pulse shape measured for a particular irradiation using a streak camera sampling a portion of the 0.26 μm laser light. Also shown is the smoothed fit used as input to calculations. The plots of Fig. 15b and 15c show the measured and calculated subkilovolt x-ray emission pulses. The measured x-ray emission pulses are shorter than calculated: the plasma appears to cool considerably more rapidly than calculated. One significant factor in the cooling is demonstrated by the 1-D calculations shown for "flat" and for "spherical segment" geometries. The divergence of the blow-off plasma reduces the plasma cooling time significantly. However, even the full 2-D calculation does not predict rapid enough cooling to match the experimental emission decay. The remaining discrepancy could represent a miscalculation of the plasma cooling rate or of the recombination/emission processes in the cooling plasma.

Let us put the 0.26 μm conversion efficiency measurements into perspective with previous measurements from Argus and with the related 0.53 μm data from Novette.[12] A summary of the measured x-ray conversion efficiencies is shown in Fig. 16. Comparing the 0.53 μm measurements from Argus (low energy, small spot diameters) with the recent 0.53 μm Novette measurements (higher energy, larger spot diameters) suggests a significant energy or spot-size dependence. Comparing the Novette measurements at 0.53 and 0.26 μm wavelengths suggests a strong wavelength dependence. Both these dependences are somewhat stronger than LASNEX scaling predictions.

The Gold Disk 0.26 μm Scaling Experiment has provided a broad first look at a very attractive laser-plasma coupling regime. Conversion of 0.26 μm laser light into subkilovolt x-rays is very efficient. Thus, we can now state firmly that the low-$I\lambda^2$ discrepancy which was evident in earlier work does not imply a conversion efficiency degradation at shorter wavelengths. Further, we have indications that scaling to higher laser energies is favorable for the x-ray conversion efficiency. Suprathermal electron production is negligible in these highly collisional plasmas. This trend has been evident in several short wavelength experiments. We note, however, that larger laser systems and plasma scalelengths could lead to increased suprathermal electron production

in the future, so it is important to continue to study and monitor the hot electron processes. LASNEX modeling with slight transport inhibition (f_e=0.05) reproduces many features of the experiments. This apparent increase in f_e from earlier analyses depends on fairly subtle changes in measured x-ray fluences, so the apparent transport improvement should be considered tentative until further verified.

Some areas of this experiment indicate a need for further study. At low intensities, the x-ray conversion efficiency appears to be energy or spot-size dependent, an effect not seen in calculations. At high intensities, the effect of M-line emission on the x-ray conversion efficiency measurements needs to be determined. For 10-50 keV x-rays, the calculated emission is much higher than that measured, suggesting a need for improved modeling of the heated electron distribution. We find, as in previous work[2], that the measured x-ray emission pulse decays faster than calculated, indicating difficulties with either the plasma cooling or atomic physics in a cooling plasma. Finally, the x-ray conversion increase between 0.53 and 0.26 μm now appears to be somewhat stronger than calculated.

IV. PLANS AND DESIGNS FOR AURORA KrF EXPERIMENTS

The KrF laser offers significant near-term benefits and long-term promise as an ICF driver. The basic KrF laser technology is ready for application. Start-up costs are consistent with current program funding levels. Near term benefits to be expected from developing KrF systems for ICF include: (1) enhance development of high-power excimer laser technology; (2) demonstrate KrF system viability for ICF applications; and (3) perform important ICF experiments. The KrF laser system is the most promising laser candidate identified to date to drive a megajoule laboratory facility and, ultimately, an ICF reactor. Its known and potential characteristics are very attractive: (1) near-optimum wavelength; (2) excellent match to present high-gain target designs; (3) 8-12% overall system efficiency; (4) high repetition-rate capability; and (5) attractive cost estimates. For these reasons, Los Alamos is pursuing KrF development for ICF applications.

Los Alamos has already achieved major milestones in KrF/ICF development.[13] The "Large Aperture Module" (LAM), with 1m x 1m aperture, has been constructed and successfully operated as an unstable resonator, producing its design pulse of 10 kJ, 500 ns.[14] Capability for high-efficiency operation has been demonstrated: (1) the LAM, an unoptimized initial design, has operated at >6% intrinsic (light output energy/cavity energy) efficiency and >2% overall (light output energy/wall-plug energy) efficiency;[14] (2) a Los Alamos/Math Sciences Northwest experiment showed 14% intrinsic efficiency using a Kr-rich gas mix;[15] and (3) calculated efficiencies of 16-20% (intrinsic) and 10% (overall) have been obtained[16] using modeling which corresponds well with present experiments. Finally, many aspects of the technology required for optical multiplexing have been demonstrated. Recently, for example, a 96 beam encoder assembly was automatically aligned to within 5 μrad in 8 minutes.[17] The next steps are now underway: a full multiplexed system demonstration and an end-to-end

experimental facility with 5 kJ, 5 ns pulse on target.

An artists' concept of the Aurora 5 kJ, 5 ns, 0.25 μm KrF laser system is shown in Fig. 17. Extension of the laser system prototype to target is essential for adequate demonstration of laser system's suitability for ICF, prior to design and construction of larger facilities. Operation as an experimental facility adds only moderate cost and offers significant opportunity to perform KrF-driven ICF experiments. Design parameters of the Aurora KrF experimental facility are shown in Table I.

Design of experiments is underway in several key areas. Investigation of KrF-specific coupling processes is an important ingredient in advanced target design. The KrF laser might (or might not) differ in important ways from Nd:glass lasers now in common use. For example, the KrF laser offers bandwidth which could be useful in certain advanced target designs for control of suprathermal electron generation. Also, the KrF architecture is drammatically different from that of Nd:glass lasers, so the beam quality, and thus the behavior of thermal filamentation, might be quite different than our experience to date would indicate. Other areas being examined are long scalelength laser-plasma coupling, hohlraum physics, and fluid instabilities.

A simplified view of plasma parameter space[18] is shown in Fig. 18 to indicate roughly the conditions which should be achievable using Aurora. The abscissa is related to the plasma temperature; the ordinate is the plasma size relative to the laser wavelength. In this parameter space, plasma process thresholds can be plotted as an indication of where the instabilities are likely to occur. Generally, instabilities become more virulent in larger, more strongly heated plasmas, upward and to the right in the figure. Reactor plasmas differ from those of present-day experiments mainly in their greater spatial scale, caused by larger energies, targets, and pulse durations. Aurora can access useful new regions of parameter space because of its short wavelength, high energy, and long pulse duration.

Determining the behavior of fluid instabilities in an ablating system is one of the great challenges for ICF experiments. Initial experiments[19] at the Naval Research Laboratory and the Rutherford-Appleton Laboratory have shown great promise for this area of research. Calculated accelerations of planar foils using Aurora parameters show (Fig. 19) attractive acceleration histories. Pressures of 20-40 Mb lead to acceleration to velocities exceeding 2×10^7 cm/sec while maintaining the dense part of the foil above 1 g/cc. Estimates suggest more than 9 "classical" Rayleigh-Taylor e-foldings for 20 μm perturbation wavelength. This should be sufficient for determining growth rates experimentally, even if the growth is below classical. It should also be sufficient to allow study of the nonlinear regime and turbulent mixing.

V. SUMMARY AND CONCLUSIONS

Let us open this section with a glimpse of the distant future: calculated plasma profiles[20] for a gold disk irradiated with a 10 MJ, 23 ns, 0.25 μm pulse (Fig. 20). LASNEX predicts that the steepening which occurs in present experimental plasmas

will persist at reactor scale. This has important consequences for the performance and coupling physics of reactor targets. We calculate a hot corona (several keV) and an x-ray conversion efficiency of about 60-65% at $3x10^{14}$ W/cm^2.

The results of this work are summarized in the updated overview of x-ray conversion measurements, shown in Fig. 21. The new, 6-beam small-sphere data from the LANL/LLE Plasma Dynamics Experiment agree well with earlier planar experiments from Argus (LLNL). However, a significant new group of experimental points from 24-beam Omega and Novette suggest a significant increase in x-ray conversion efficiency, perhaps due to the use of higher energy and larger targets. Although this change was not predicted by LASNEX calculations, the change can be fit using less-inhibited electron thermal transport and somewhat improved modeling at low intensities. It is also noteworthy that the low-intensity roll-off seen in previous experiments is not apparent in the recent large-target experiments, and thus now appears to be target-size (spot-size) dependent.

Our understanding of the physics and scaling of high-Z plasma processes has improved considerably. Laser-plasma coupling at 0.26 μm wavelength now appears to be very favorable: x-ray conversion is quite efficient and suprathermal electron fractions and temperatures are very low. We have tested, for the first time, the LASNEX predictions for energy penetration and x-ray emission depth in high-Z plasmas, and have found excellent agreement. Initial plans and designs for Aurora experiments appear quite promising.

A number of issues remain to be assessed and studied. The x-ray conversion efficiency data now suggests scaling dependence upon target-size (or laser energy) and, to a lesser extent, wavelength, which is stronger than predicted. Certain details of the sub-keV x-ray spectrum and time-dependence remain uncertain, with some differences apparent between one experiment and another or between one diagnostic and another. If the high-resolution subkilovolt spectrum is correct, dielectronic recombination may be playing an important role in reducing the ionization states and softening the x-ray spectra. Calculations overestimate the hard (10-50 keV) x-ray emission at high intensities by a large factor, suggesting that a sub-Maxwellian heated electron distribution might be important. These areas need continued experimental and calculational work.

ACKNOWLEDGEMENTS

The authors are grateful for the contributions of many coworkers and the laboratories which have made this work possible.

We thank our Los Alamos colleagues, W. Gula, M. Mahaffy, J. Norton, and J. Saltzman for assistance in the use of LASNEX, and J. Cobble and G. Stradling for their contributions to the Plasma Dynamics Experiment. The support of D. Cartwright, D. Giovanelli, and S. Rockwood is appreciated.

We thank the University of Rochester Laboratory for Laser Energetics for cooperation and the use of OMEGA. Thanks are due to M. Richardson, P. Jaanimagi

(Lawrence Berkeley Laboratory), S. Letzring, R. Marjoribanks, and F. Marshall for their helpful collaboration. The support of J. Soures and R. McCrory is appreciated.

We appreciate the cooperation of Lawrence Livermore National Laboratory, and particularly R. Kauffman, E. M. Campbell, and E. Storm, in providing the Novette data. We thank B. Lasinski, D. Bailey, K. Estabrook, and W. Kruer for valuable discussions; and R. Kauffman, R. P. Drake, H. Kornblum, J. Smith (Aracore, Inc.), and R. Turner for their contributions to the 0.26 μm Scaling Experiment.

We thank members of the Target Fabrication, Diagnostics, and Laser Operations groups at each of the laboratories for their essential contributions.

The support of the U.S. Department of Energy is appreciated.

REFERENCES

[1]M. D. Rosen, D. W. Phillion, V. C. Rupert, W. C. Mead, W. L. Kruer, J. J. Thomson, and K. G. Tirsell, Phys. Fluids **22**, 2020 (1979).

[2]W. C. Mead, E. M. Campbell, K. G. Estabrook, R. E. Turner, W. L. Kruer, P. H. Y. Lee, B. Pruett, V. C. Rupert, K. G. Tirsell, G. L. Stradling, F. Ze, C. E. Max, M. D. Rosen, and B. F. Lasinski, Phys. Fluids **26**, 2316 (1983).

[3]G. B. Zimmerman, Lawrence Livermore National Laboratory Rpt. No. UCRL-75881 (1974); G. B. Zimmerman and W. L. Kruer, Comm. Plasma Phys. and Contr. Fusion **2**, 85 (1975).

[4]P. D. Goldstone, R. H. Day, G. Eden, F. Ameduri, W. C. Mead, S. R. Goldman, M. C. Richardson, R. L. Keck, W. Seka, G. Pien, J. M. Soures R. L. McCrory, and J. Knauer, Bull. Am. Phys. Soc. **29**, 1318 (1984); R. S. Marjoribanks, *et al.*, *loc. cit.*; S. A. Letzring, *et al.*, *loc. cit.*

[5]R. L. Kauffman, R. P. Drake, R. E. Turner, B. F. Lasinski, G. Tirsell, W. C. Mead, and E. Stover, Bull. Am. Phys. Soc. **29**, 1183 (1984).

[6] O. Willi, Z. Q. Lin, and P. T. Rumsby, Rutherford-Appleton Laboratory Rpt. No. RL-83-043, p. 4.9 (1983); M. J. Herbst, J. A. Stamper, R. R. Whitlock, R. H. Lehmberg, and B. H. Ripin, Phys. Rev. Lett. **46**, 328 (1981).

[7]M. G. Haines, Phys. Rev. Lett. **47**, 917 (1981).

[8]R. G. Evans, Rutherford-Appleton Laboratory Rpt. No. RL-82-059, p.3.25 (1982).

[9] A. B. Langdon, Phys. Rev. Lett. **44**, 575 (1980).

[10]J. R. Albritton, Phys. Rev. Lett. **50**, 2078 (1983).

[11]T. J. Goldsack, J. D. Kilkenny, B. J. MacGowan, P. F. Cunningham, C. S. Lewis, M. H. Key, and P. T. Rumsby, Phys. Fluids **25**, 1634 (1982); A. Hauer, W. C. Mead, O. Willi, J. D. Kilkenny, D. K. Bradley, S. D. Tabatabaei, and C. Hooker, Phys. Rev. Lett. **53**, 2563 (1984); M. D. Rosen, Comm. Plasma Phys. and Contr. Fusion **8**, 165 (1984), and references therein.

[12]E. M. Campbell, R. P. Drake, R. E. Turner, D. W. Phillion, W. L. Kruer, B. F. Lasinski, C. L. Wang, K. G. Estabrook, and C. W. Hatcher, 14th Ann. Anomalous Absorption Conf. , Charlottesville, Va., May 6-11, 1984.

[13]L. A. Rosocha, P. S. Bowling, M. D. Burrows, M. Kang, J. A. Hanlon, J. McLeod, and G. W. York, Jr., To be published in Lasers and Part. Beams ; L. A. Rosocha, P. D. Goldstone, and R. Kristal, Submitted to Conf. on Lasers and Electro-Optics '86, June, 1986.

[14]G. W. York, Jr., S. J. Czuchlewski, L. A. Rosocha, and E. T. Salesky, Conf. on Lasers and Electro-Optics '85, paper THL3, May, 1985.

[15]E. T. Salesky and W. D. Kimura, IEEE Journ. of Quant. Elec. **QE-21**, 1761 (1985).

[16]E. T. Salesky, Priv. comm., 1984; M. Tanimoto, A. Yaoita, I. Okuda, and Y. Owadano, Jap. Journ. Appl. Phys. **24**, L311 (1985).

[17]B. L. Kortegaard, Soc. Photo Inst. Eng. **534**, 159 (1985).

[18]W. L. Kruer and W. C. Mead, Priv comm., 1982.

[19]R. R. Whitlock, M. H. Emery, J. A. Stamper, E. A. McLean, S. P. Obenschain, and M. C. Peckerar, Phys. Rev. Lett. **52**, 819 (1984); J. Grun, M. H. Emery, S. Kacenjar, C. B. Opal, E. A. McLean, S. P. Obenschain, B. H. Ripin, and A. Schmitt, Phys. Rev. Lett. **53**, 1352 (1984); B. J. MacGcwan, J. D. Kilkenny, A. P. Fews, D. L. Henshaw, M. H. Key, P. T. Rumsby, and W. T. Toner, Rutherford-Appleton Laboratory Rpt. No. RL-83-043, p. 6.13 (1983).

[20]S. R. Goldman and W. C. Mead, Submitted for publication.

Table I. Parameters of the Aurora KrF experimental facility.

WAVELENGTH	0.25μm
ENERGY	5–8kJ
PULSE DURATION	5ns
PULSE SHAPE	1 TO 2 STEPS
MIN. SPOT DIA.	200μm
ASE + PREPULSE	<50mJ
BANDWIDTH	~0.1%
BEAM CLUSTERING	
# BUNDLES	1
BUNDLE f#	~2
# BEAMLETS	48
BEAMLET f#	26
COMPLETION DATE	MID-FY87

OPTIONS: ENHANCED BANDWIDTH; ISI
HIGHER ENERGY (2 BUNDLES, 96 BEAMLETS)
2ns PULSE

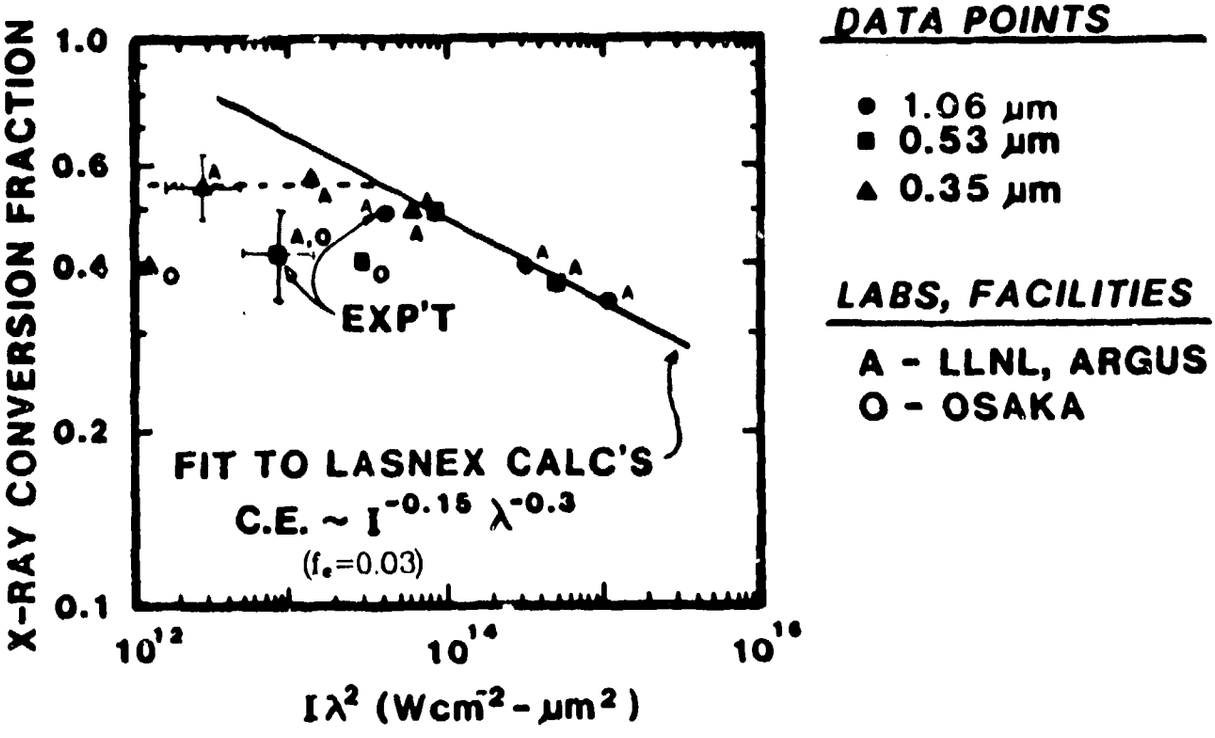

Fig. 1. Summary of x-ray conversion efficiency data and calculations for gold disk targets, as of 1983. Irradiations used 3-200 J, 600-1000 ps Gaussian pulses. The line is a power-law fit to LASNEX calculations over roughly the same parameter range as the data. X-ray conversion efficiency increases at shorter laser wavelengths, at least when $I\lambda^2 > 10^{14}\ W cm^{-2}\ \mu m^2$.

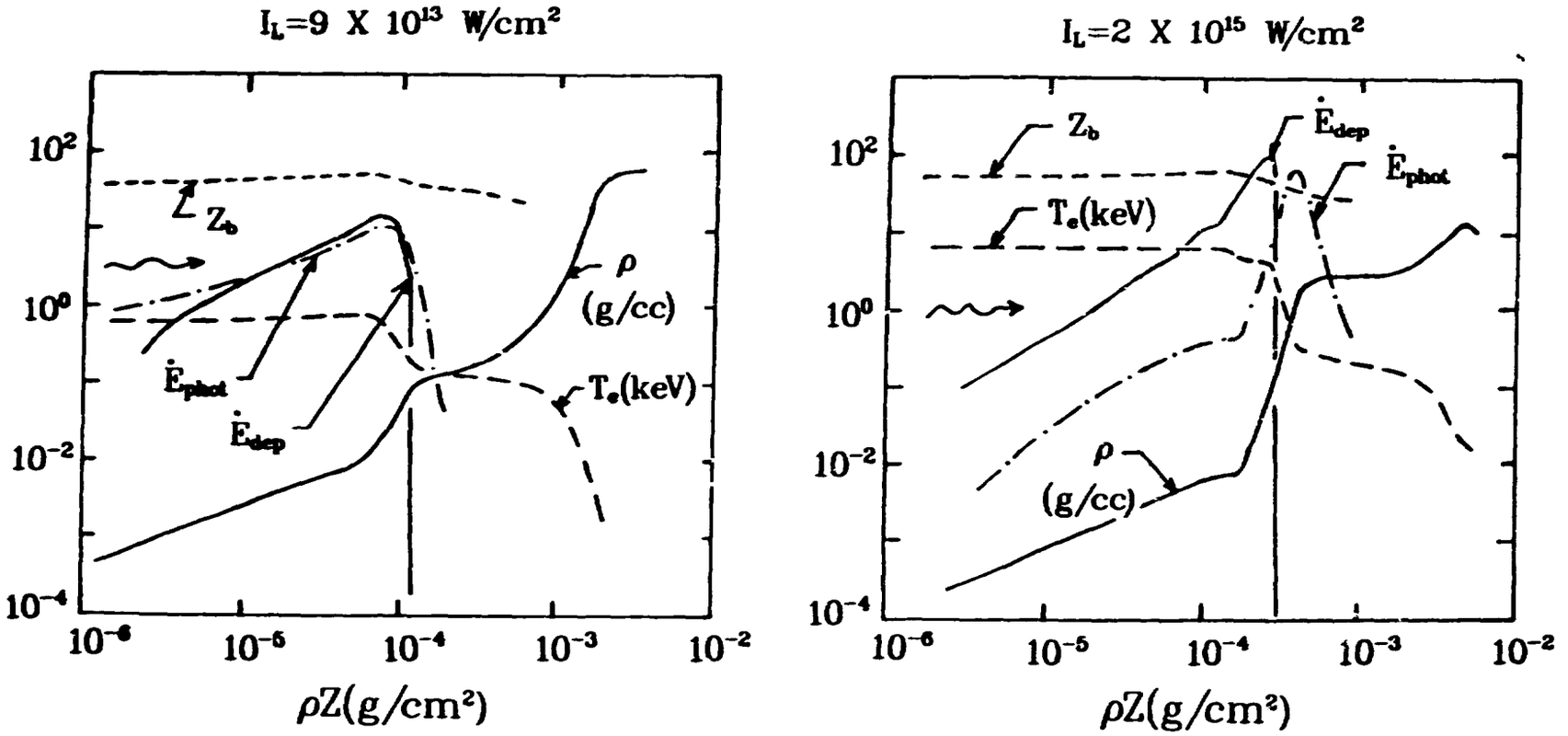

Fig. 2. Caiculated (f_e=0.05) plasma profiles for gold disk targets at 0.25 μm wavelength, about 2 kJ energy, and 1 ns pulse duration. The profile characteristics change significantly between 10^{14} and 10^{15} W/cm^2, leading to sharper gradients at higher intensities and providing several observable signatures.

MAIN MEASUREMENTS

SUB–keV X–RAY EMISSION

ABSOLUTE, TIME–RESOLVED, HIGH RESOLUTION keV EMISSION (M–LINES)

TIME–INTEGRATED, TIME RESOLVED X–RAY IMAGES

IRRADIATION CONDITIONS

$\lambda_L = 0.35\mu m$

$\tau_L \simeq 600ps$ FWHM

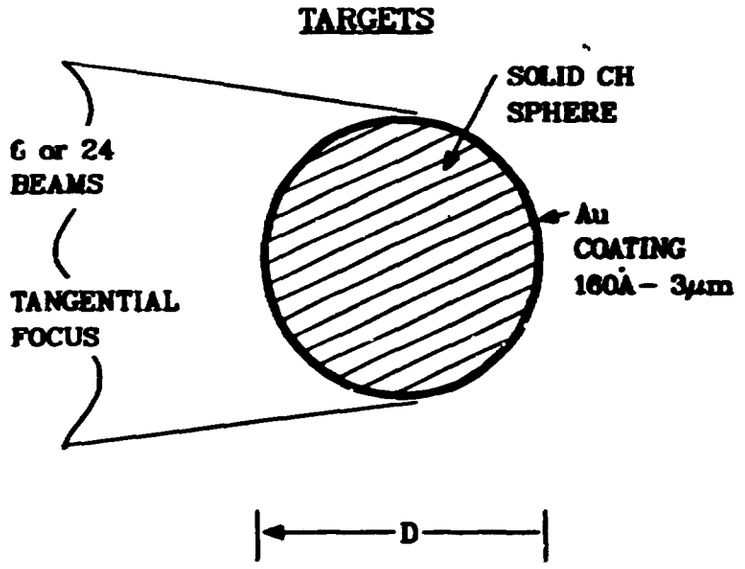

INTENSITY (W/cm^2)	$5 \cdot 10^{12}$	$4 \cdot 10^{13}$		$4 \cdot 10^{14}$		$3 \cdot 10^{15}$
# OF BEAMS	24	6	24	6	24	24
ENERGY (J)	250	250	1800	250	1700	1600
TARGET D (μm)	1650	600	1600	200	450	140

Fig. 3. Scheme of the High-Z Plasma Dynamics Experiment. Gold-on-CH spheres were used to probe energy penetration and x-ray generation processes.

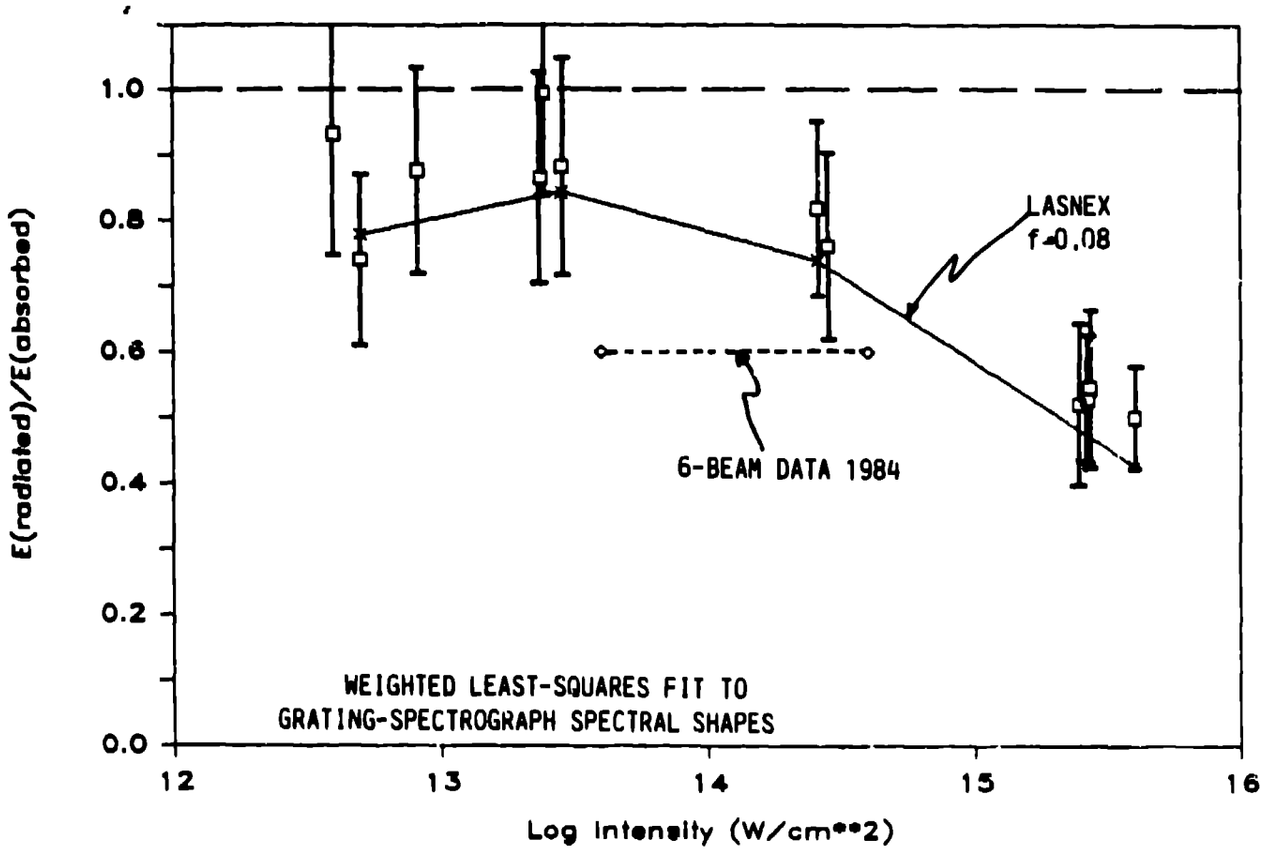

Fig. 4. X-ray conversion efficiency *vs.* intensity for Au spheres at λ_L=0.35 μm, τ_L=600 ps. The 6- and 24-beam irradiations yielded different x-ray conversion efficiency at low intensity. The 24-beam irradiations agree very well with calculations using f_e=0.08.

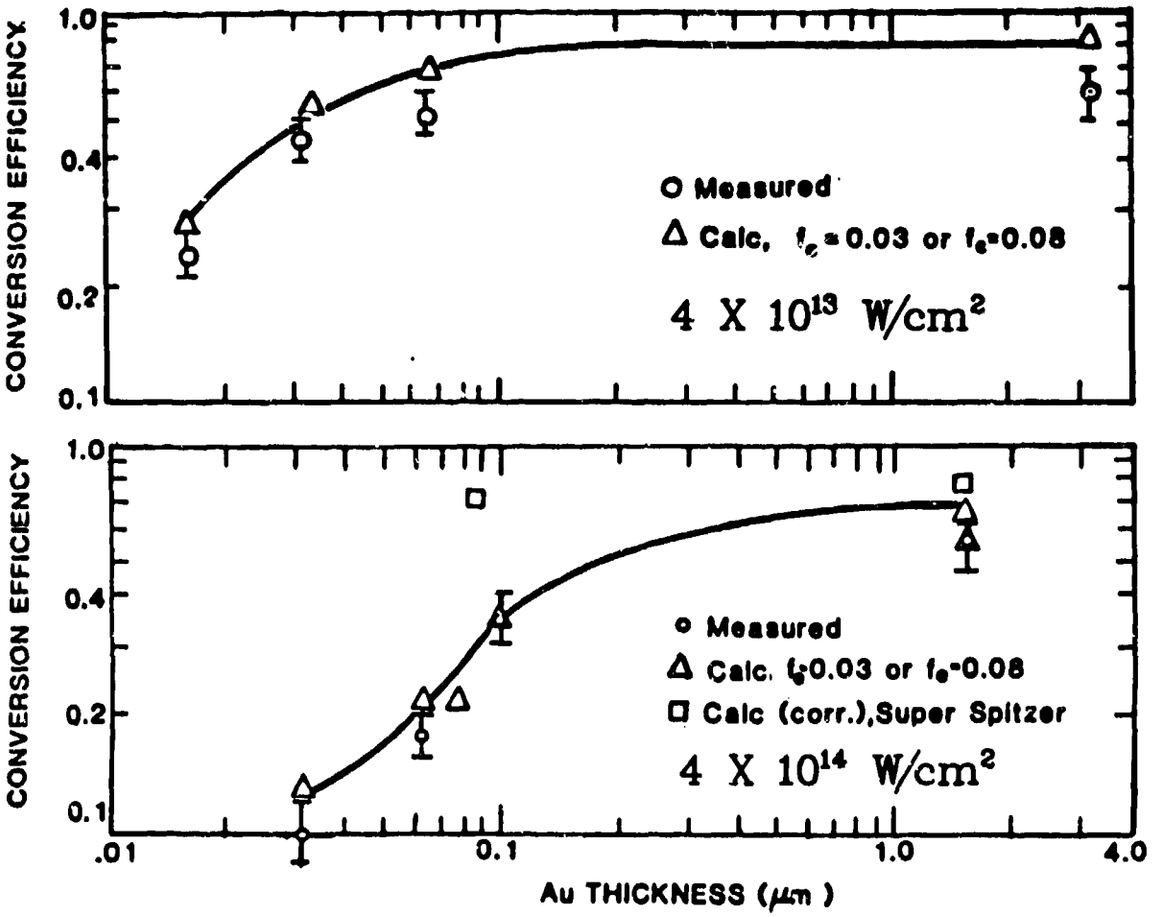

Fig. 5. Predicted and observed x-ray conversion efficiencies *vs.* gold coating thickness for Au-on-CH spheres, 6-beam irradiations. Curves are smooth lines through the f_e=0.08 calculations. Measured x-ray emission fall-off is in good agreement with that calculated, indicating that energy penetration and x-ray emission regions correspond well with predictions.

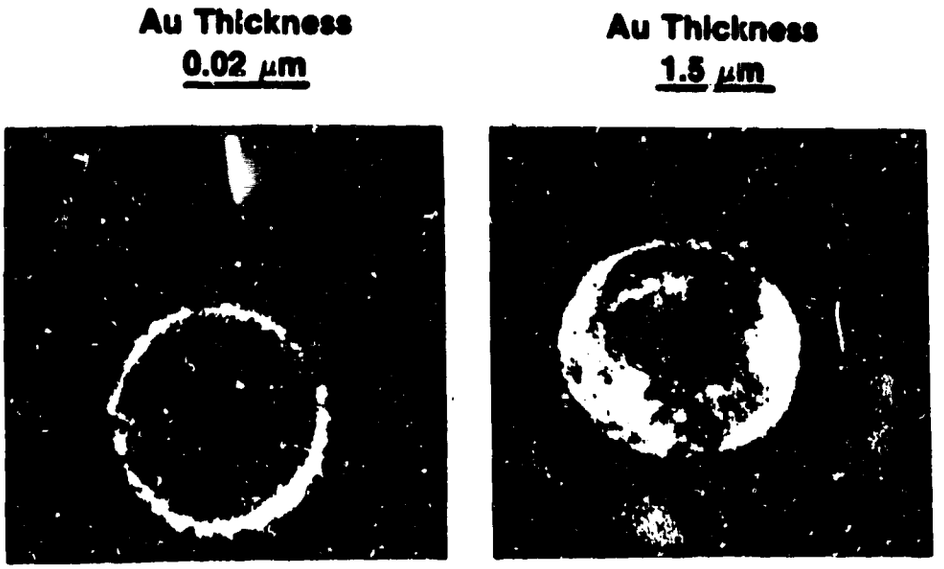

Fig. 6. X-ray images (1-3 keV) for Au-on-CH spherical targets with 6-beam irradiations. Target diameter of 600 μm and 6-beam irradiation led to 4x10^{13} W/cm^2 intensities. Resolution of the Kirkpatrick-Bacz microscope was about 5 μm. Filamentary structure is evident in the emission, particularly for the targets with thin gold coatings.

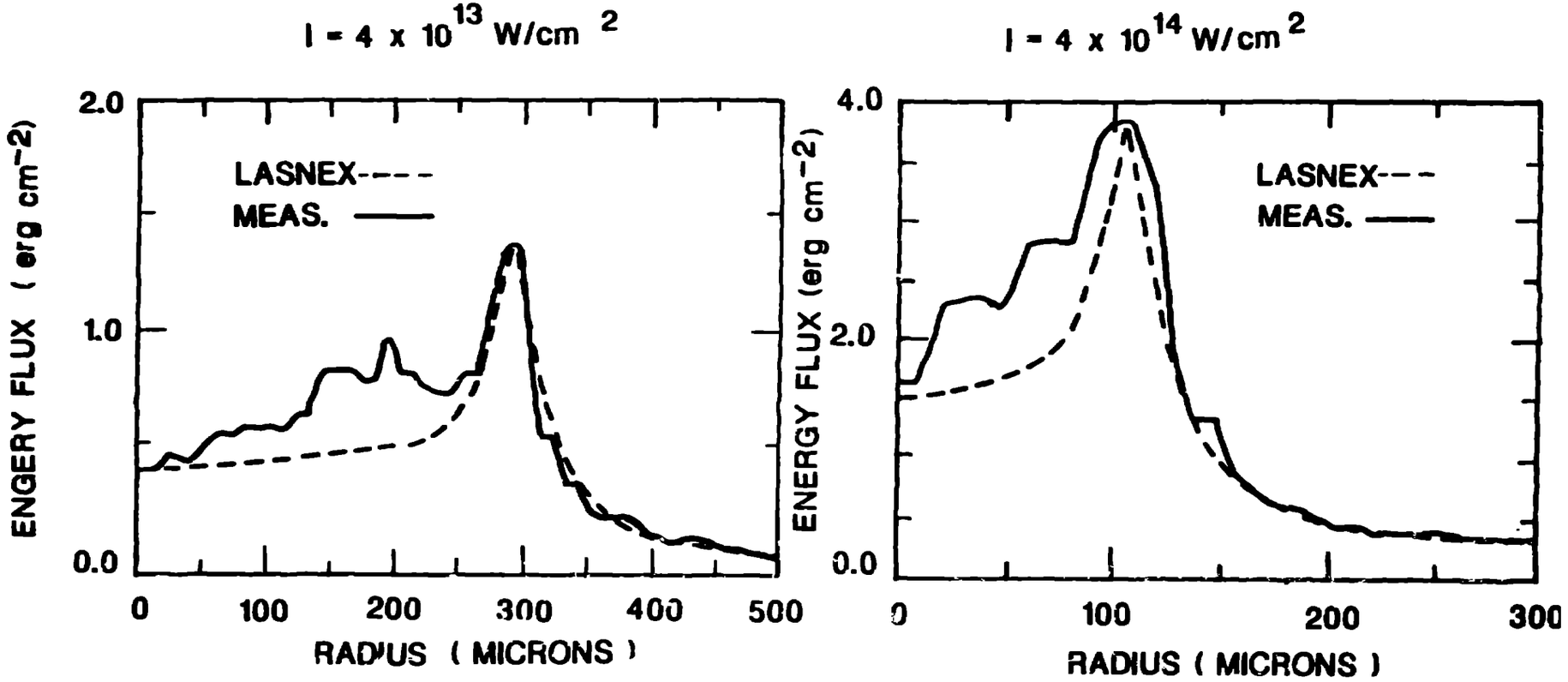

Fig. 7. Measured and calculated radial traces of x-ray images. To plot the measurements, background was subtracted and peak was normalized to match the calculations. Observed emission profiles, including the relative limb brightness and extent, are comparable to those calculated.

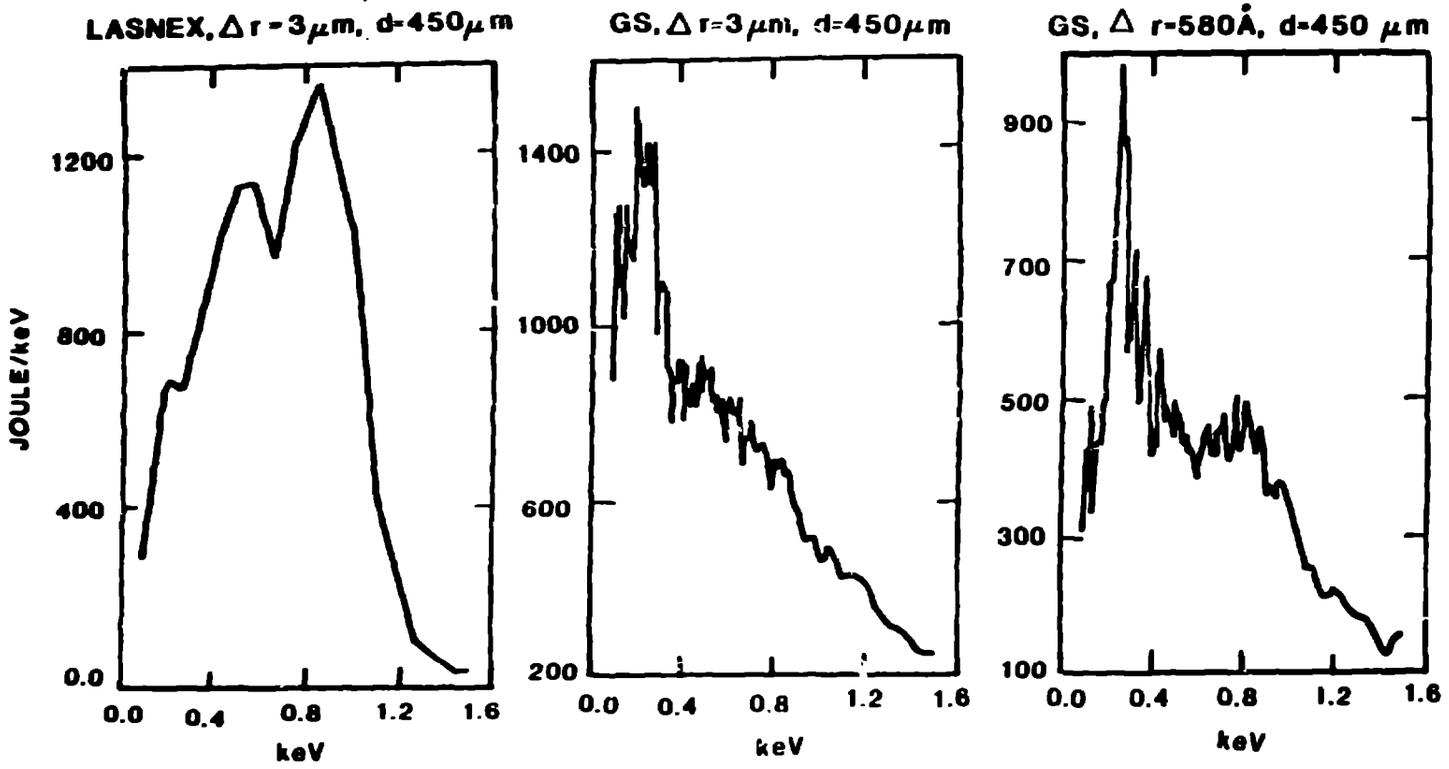

Fig. 8. LASNEX-calculated and Grating-Spectrograph-measured (GS) soft x-ray spectra at 4x10^{14} W/cm^2 intensity. Measurements show relatively weaker N-manifold (0.8-1.2 keV) and stronger O-manifold (0.4-0.8 keV) than predicted.

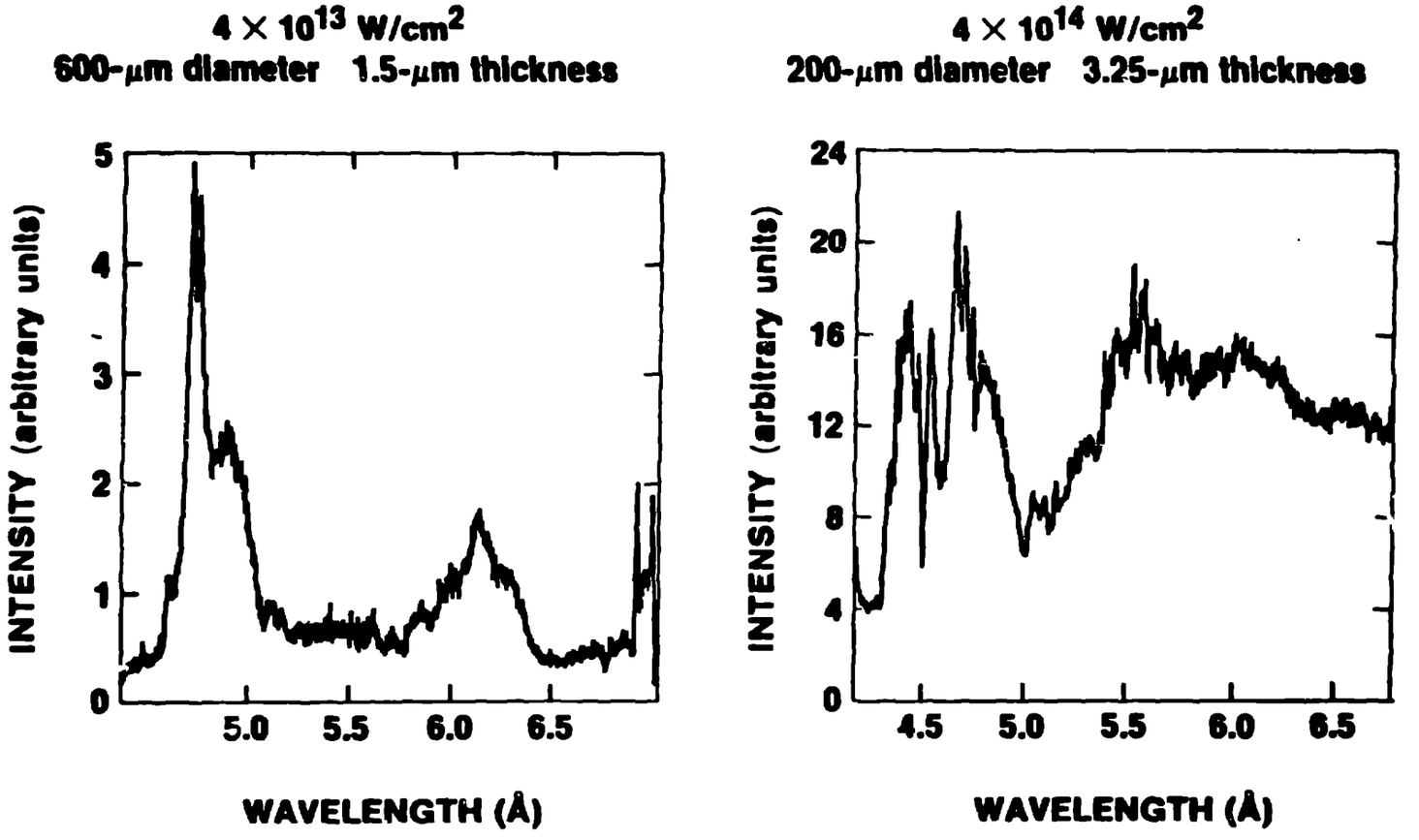

Fig. 9. Spectra in the M-line region (the photon energy in keV is 12.4 divided by the wavelength in Angstroms; thus, 5 Å corresponds to about 2.5 keV), obtained using a Gypsum crystal spectrograph. The increase of the M-line emission for the higher intensity irradiations is evident (the "arbitrary units" are the same for both portions of the figure).

IRRADIATION CONDITIONS

f/4 FOCUSING LENS

$\lambda_L = 0.26\mu m$

$\tau_L \simeq 1$ ns, GAUSSIAN

$E_L = 0.5$ TO 1.6 kJ

$D_S = 300$ TO 1500 μm

$I_L = 9 \times 10^{13}$ W/cm^2

TO

2×10^{15} W/cm^2

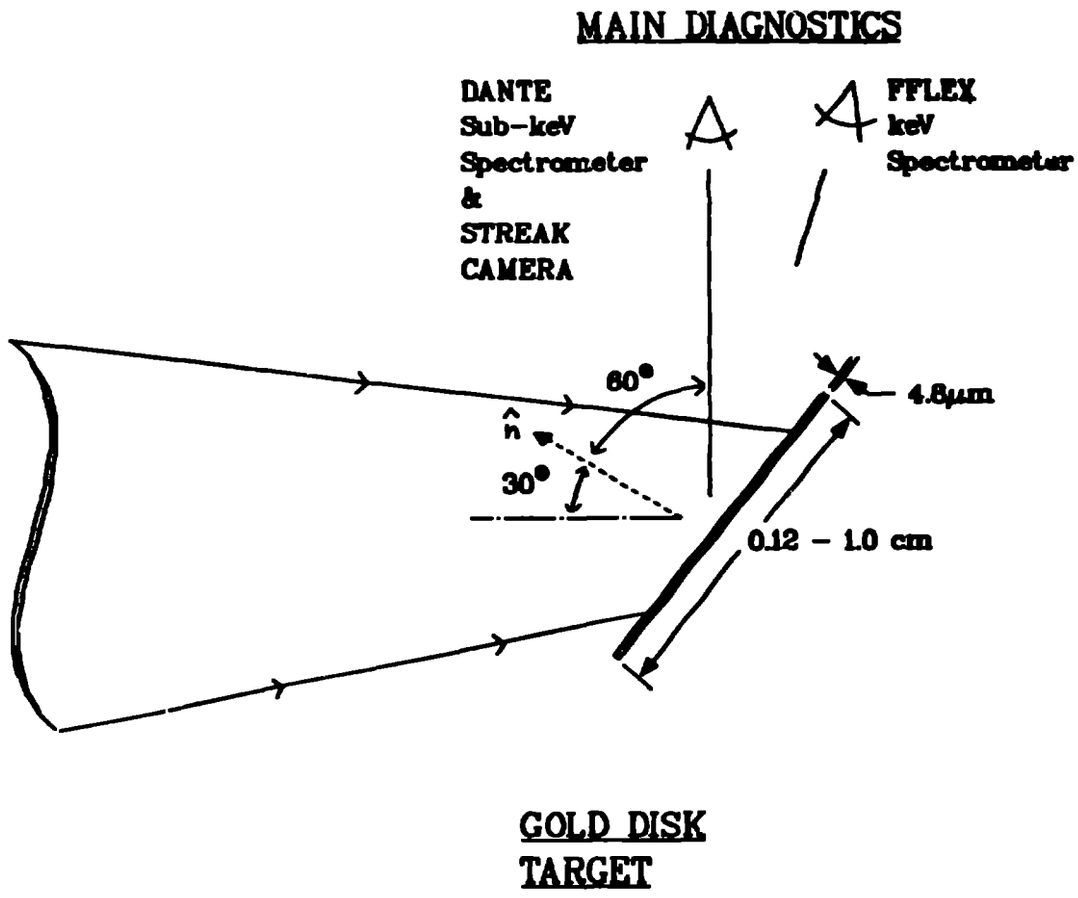

Fig. 10. Scheme of the Gold Disk 0.26 μm Scaling Experiment. The Au disk target was tilted at 30° to the incident beam direction, allowing the soft x-rays to be observed at 60° to the target normal.

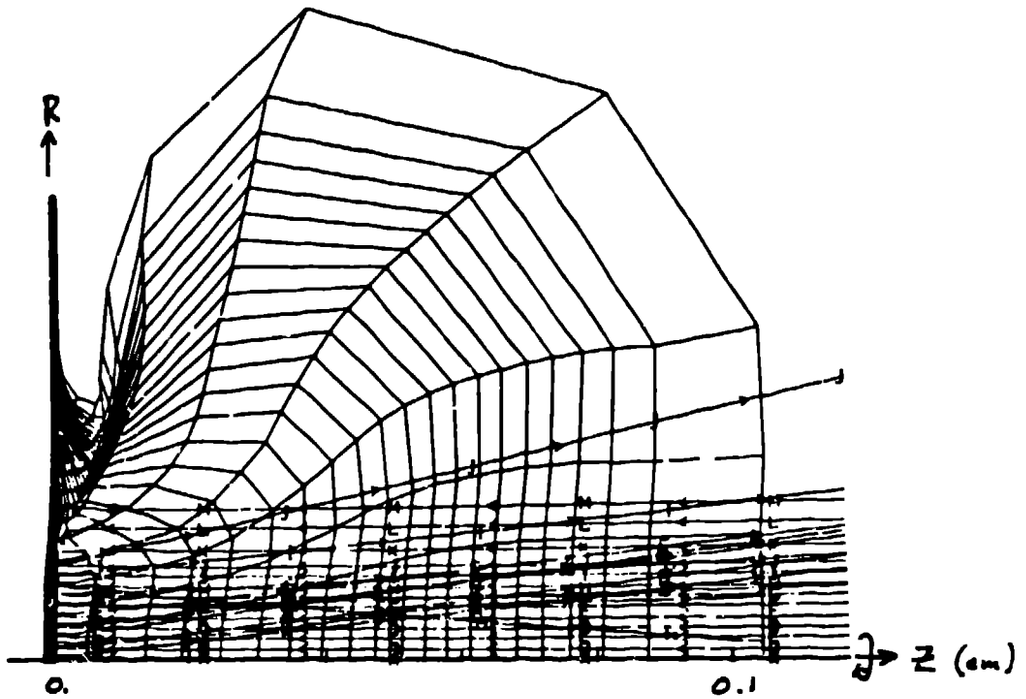

Fig. 11. Snapshot of 2D LASNEX calculation at the time of the peak of the laser pulse for λ_L=0.26 μm, τ_L=1 ns, E_L=1.3 kJ, I_L=2x10^{15} W/cm^2, using f_e=0.05.

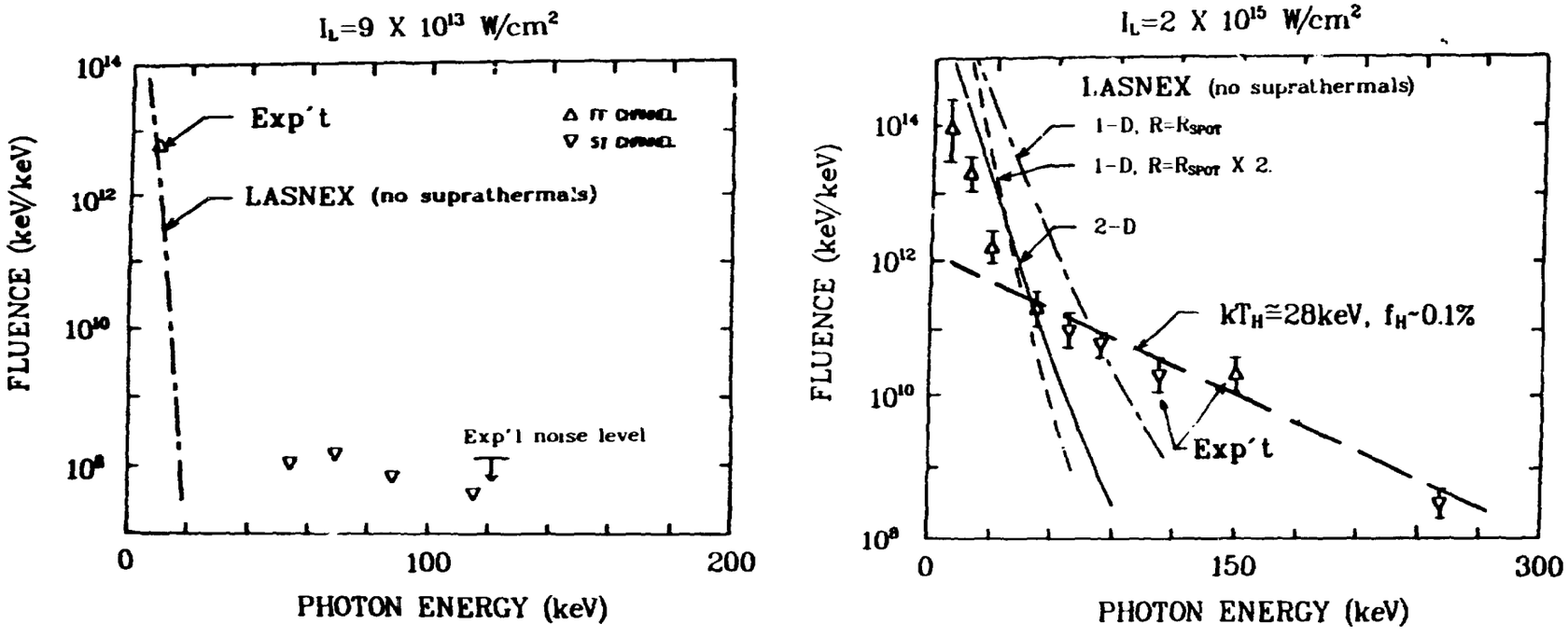

Fig. 12. Measured and calculated hard x-ray spectra, indicating cool coronas and very low suprathermal populations for this experiment at 0.26 μm.

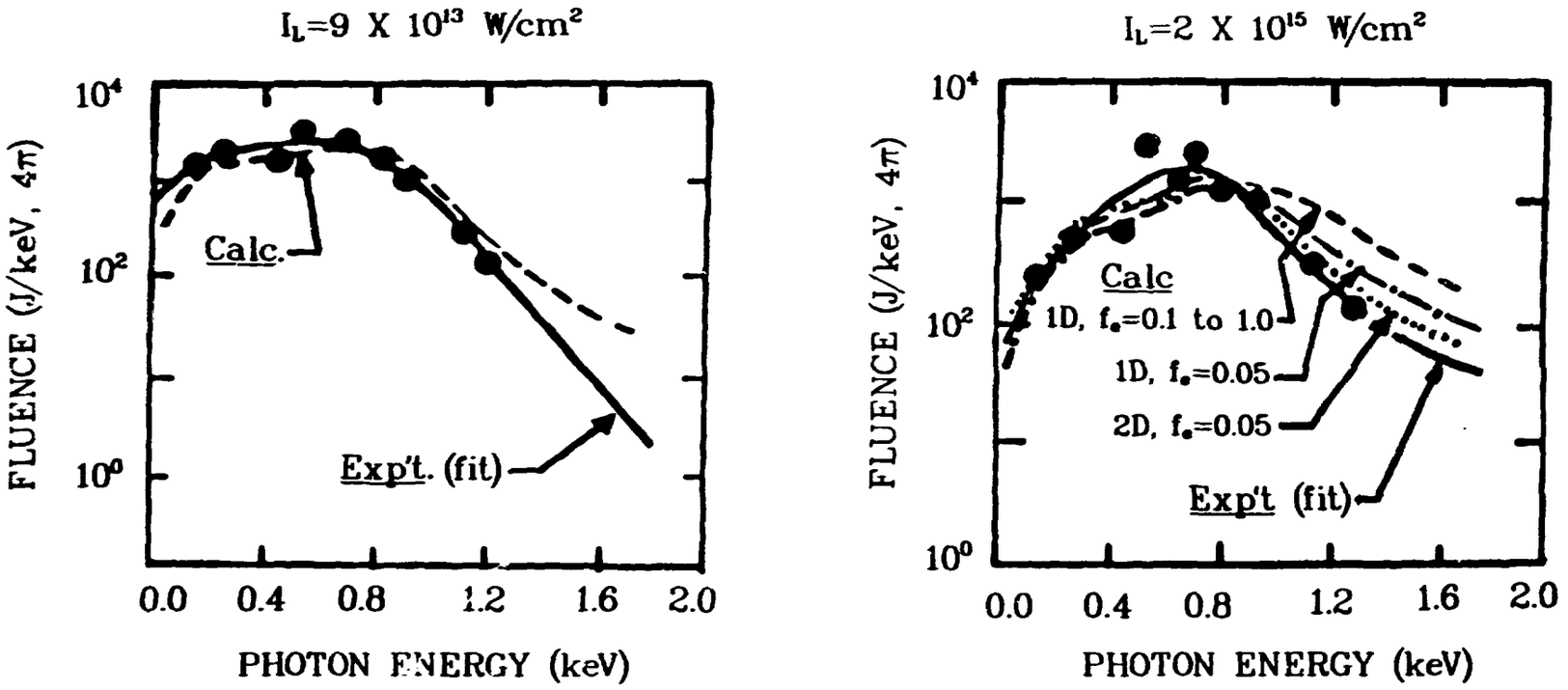

Fig. 13. Broad-band soft x-ray spectra. Observed spectra agree well with calculations using mildly inhibited transport (f_e=0.05).

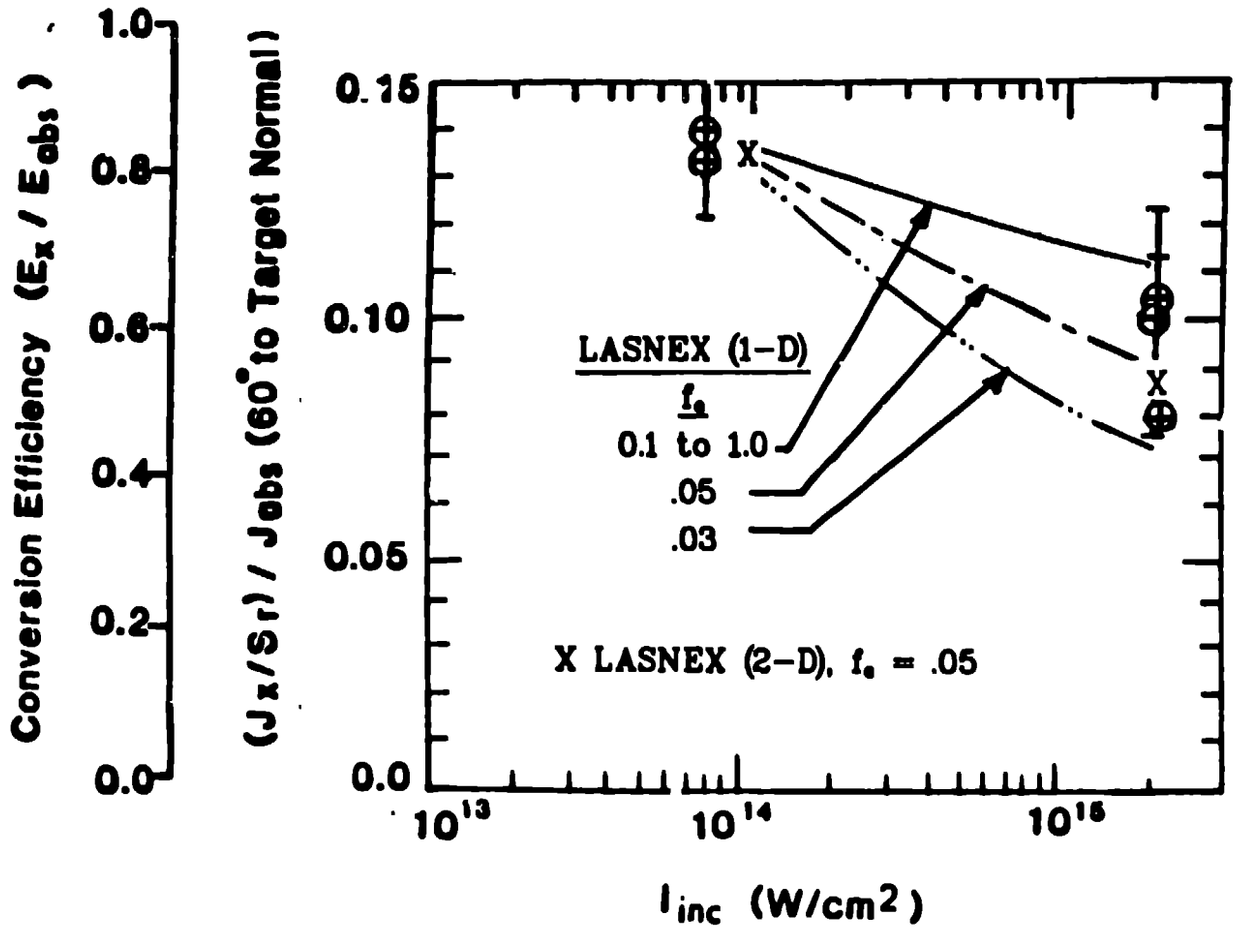

Fig. 14. X-ray emission data and calculations. Experimental points are integrated over the Dante unfold for the 0.-1.8 keV region. Calculated points were obtained using the TDG code in conjunction with the LASNEX 2D calculations to evaluate the emission at 60°, as well as to integrate the total emission and provide the conversion efficiency scale.

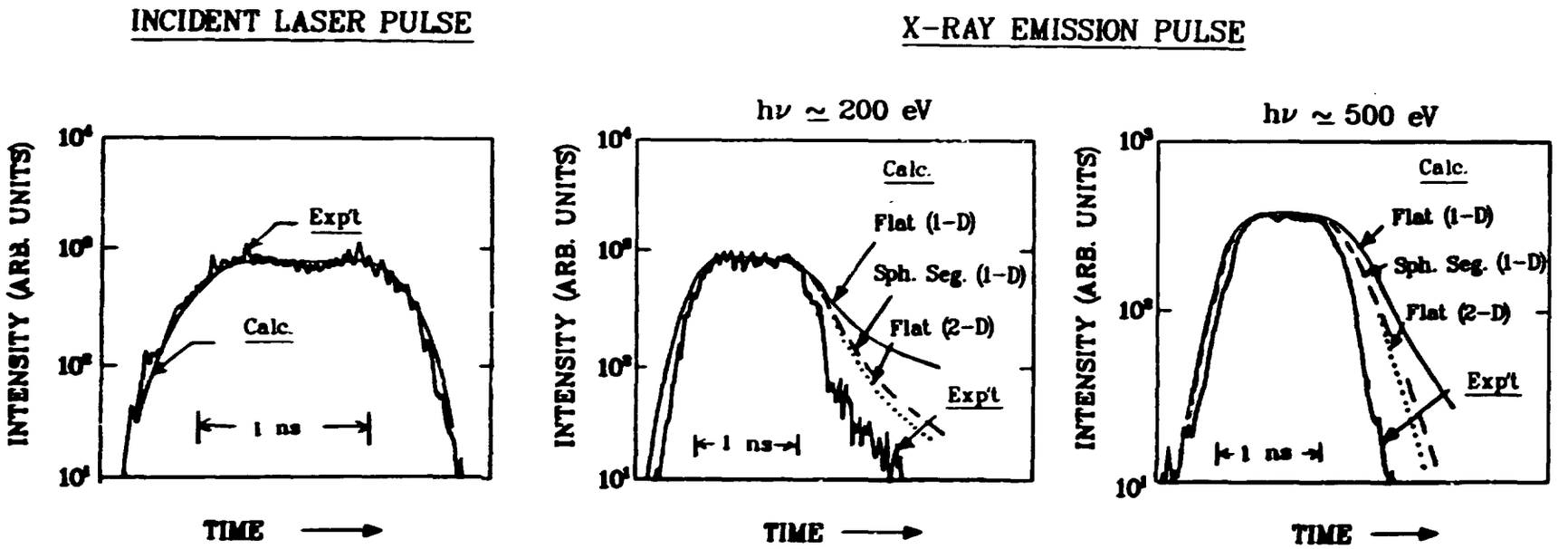

Fig. 15. Temporal shapes for incident laser pulse and x-ray emission pulses. Using the incident pulse shown as input, the calculated x-ray pulses are somewhat longer than those observed, mainly as a result of a considerably slower decay.

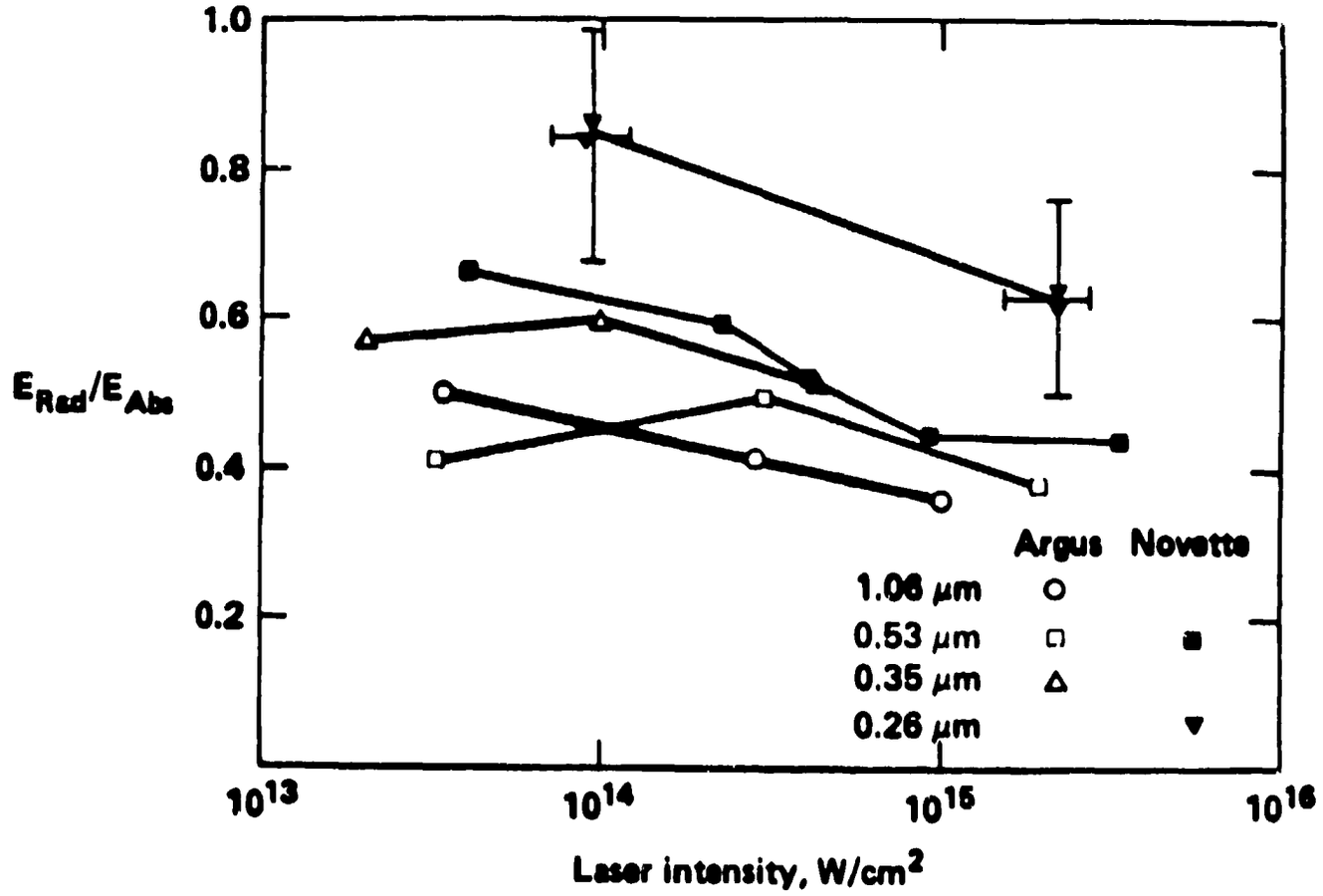

Fig. 16. Measured x-ray conversion efficiencies.

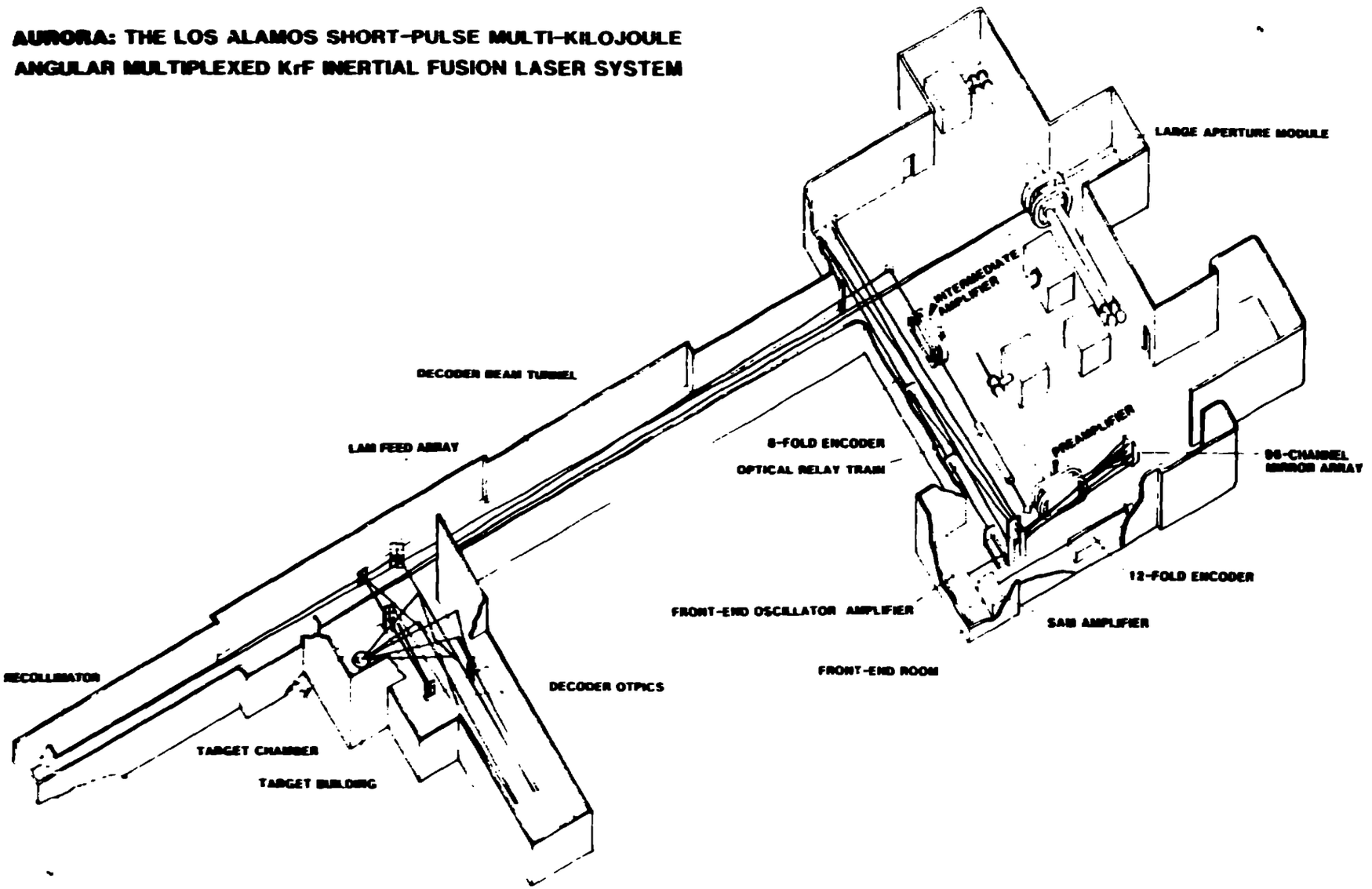

Fig. 17. Artist's concept of the Aurora KrF laser system.

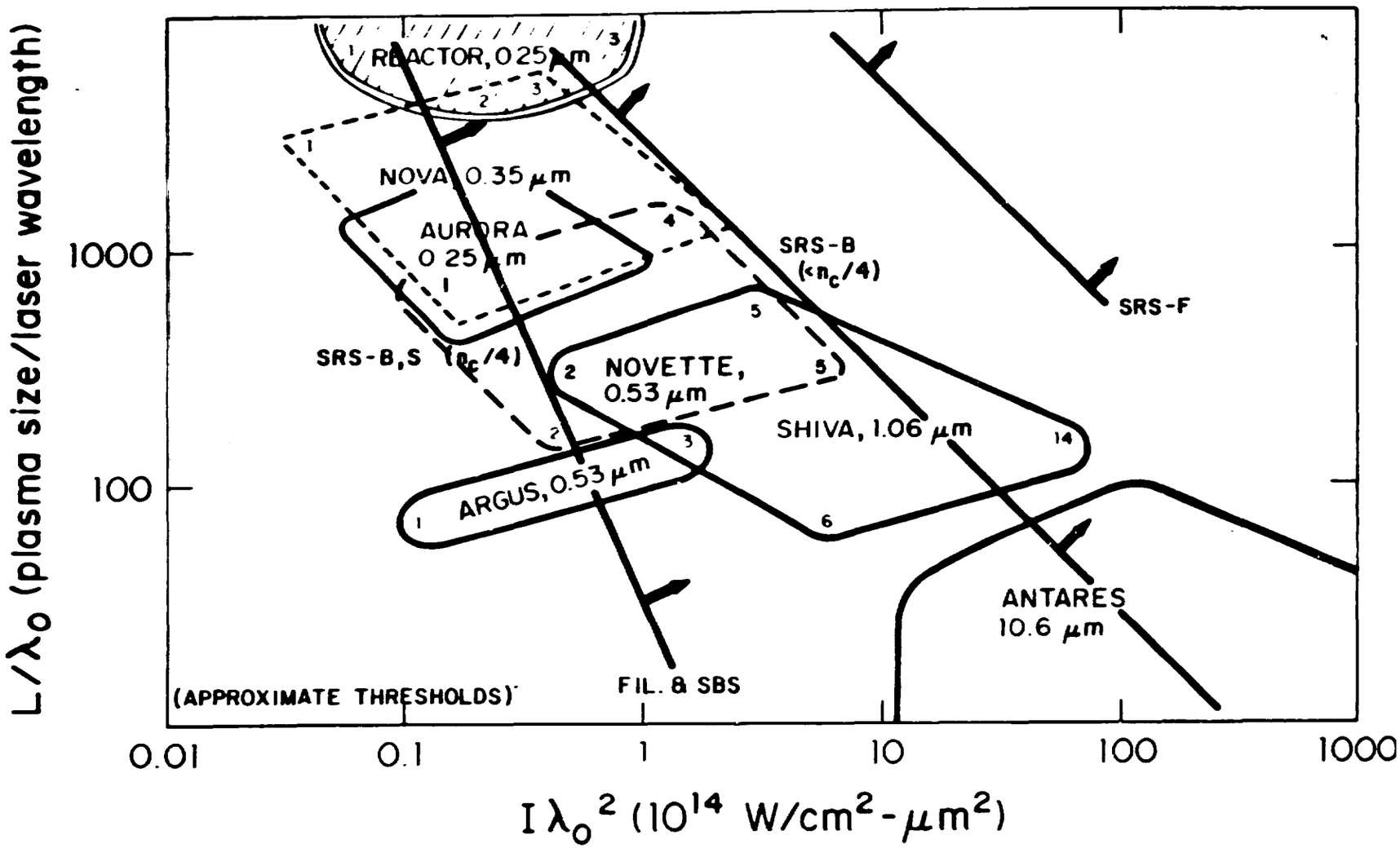

Fig. 18. Simplified view of plasma parameter space. Numbers in the corners of the facility "boxes" indicate estimated plasma temperatures in keV. Aurora will access new and important plasma conditions.

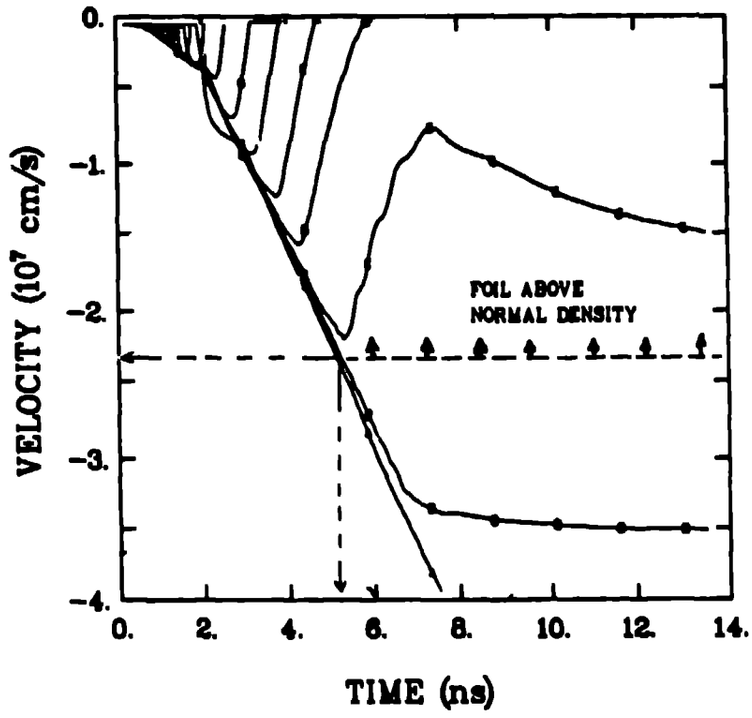

Fig. 19. Calculated velocity history for planar foil accelerated using Aurora's design parameters. Foil was initially 30 μm thick, CH. Laser pulse was 5kJ, 5 ns flat-topped (with 1 ns rise- and fall- times). Estimates show about 9 e-foldings, classically, for perturbations of 20 μm wavelength.

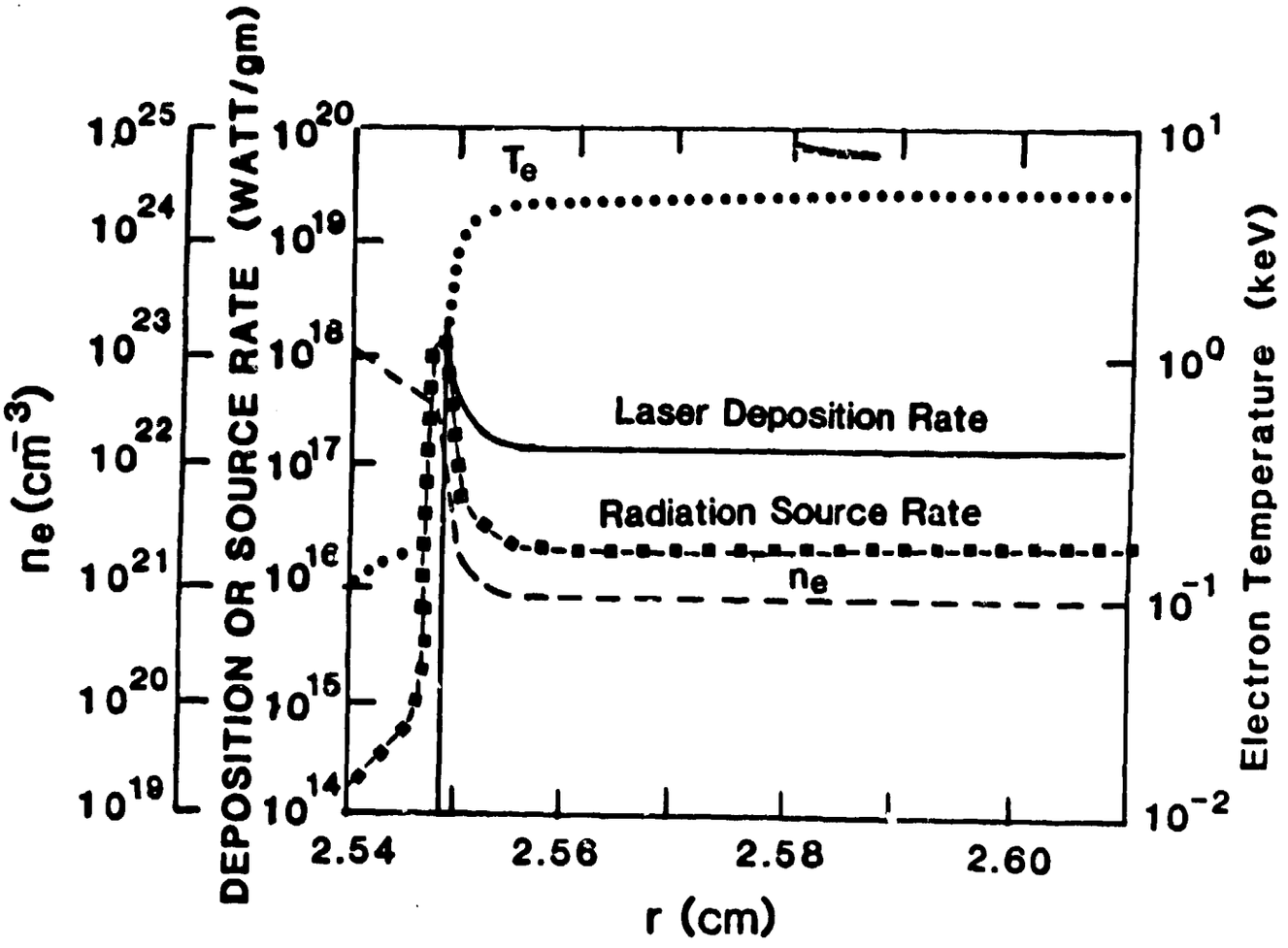

Fig. 20. LASNEX-calculated plasma profiles for 0.25 μm KrF irradiation at 10 MJ, 23 ns, 3x10^{14} W/cm^2. Plasma characteristics of current laboratory plasmas persist for future irradiation parameters: a hot corona, strong steepening near the critical density, and calculated x-ray conversion efficiency of 60-65%.

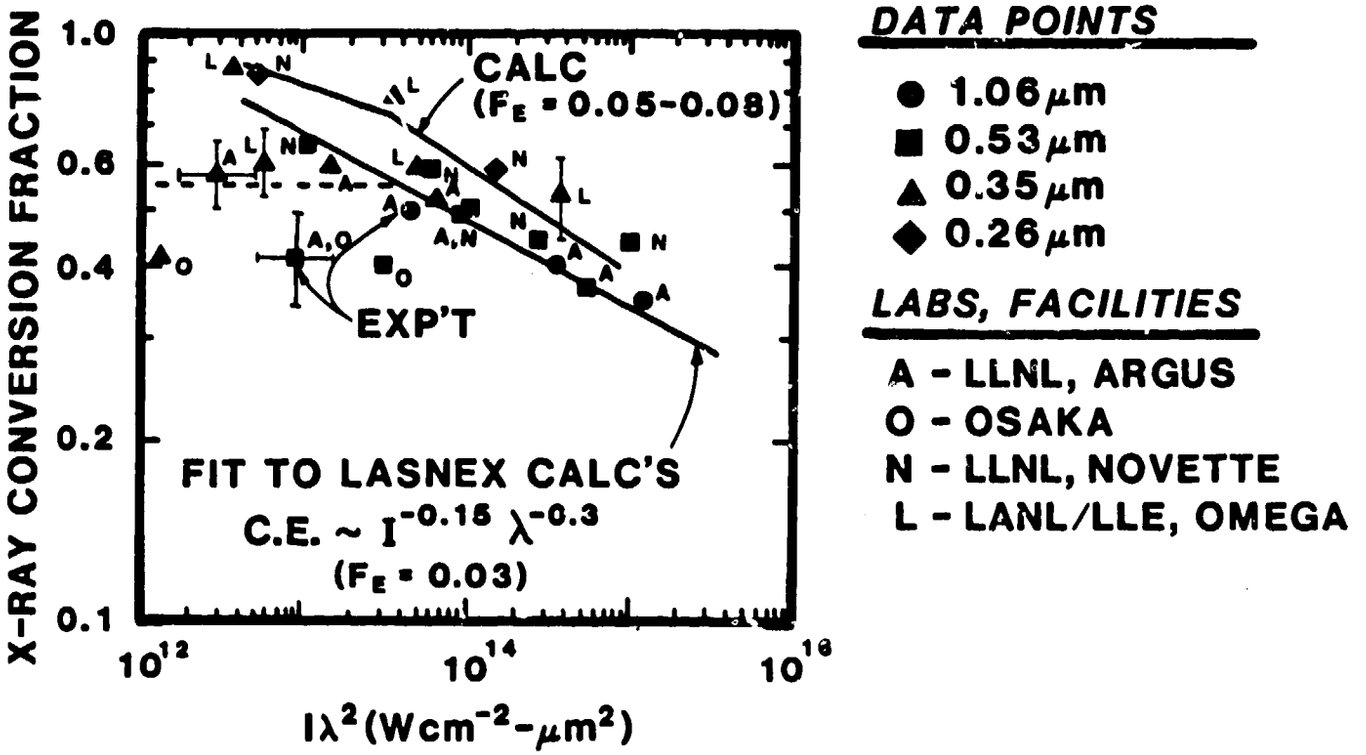

Fig. 21. Summary of x-ray conversion efficiency data, as of 1985. The data points and fit to f_e=0.03 calculations shown in Fig. 1 are reproduced here. The values inferred from the experiments analyzed in this paper (including spherical targets and irradiation energies up t· 2 kJ) have been added. The recent LASNEX calculations, using f_e=0.05-0.08 and more rigorous treatment of numerical convergence of the atomic physics modeling, lie on the upper curve shown. The overall conversion efficiency scaling is not greatly altered. However, recent data lies above previous experiments, a matter requiring further understanding.